

Hot-Jupiter Core Mass from Roche-lobe Overflow

Sivan Ginzburg^{*} and Re'em Sari

Racah Institute of Physics, The Hebrew University, Jerusalem 91904, Israel

Accepted XXX. Received YYY; in original form ZZZ

ABSTRACT

The orbits of many observed hot Jupiters are decaying rapidly due to tidal interaction, eventually reaching the Roche limit. We analytically study the ensuing coupled mass loss and orbital evolution during the Roche-lobe overflow and find two possible scenarios. Planets with light cores $M_c \lesssim 6M_\oplus$ (assuming a nominal tidal dissipation factor $Q \sim 10^6$ for the host star) are transformed into Neptune-mass gas planets, orbiting at a separation (relative to the stellar radius) $a/R_\star \approx 3.5$. Planets with heavier cores $M_c \gtrsim 6M_\oplus$ plunge rapidly until they are destroyed at the stellar surface. Remnant gas-Neptunes, which are stable to photo-evaporation, are absent from the observations, despite their unique transit radius ($5 - 10R_\oplus$). This result suggests that $M_c \gtrsim 6M_\oplus$, providing a useful constraint on the poorly-known core mass that may distinguish between different formation theories of gas giants. Alternatively, if one assumes a prior of $M_c \approx 6M_\oplus$ from the core-accretion theory, our results suggest that Q does not lie in the range $10^6 \lesssim Q \lesssim 10^7$.

Key words: planets and satellites: composition – planets and satellites: gaseous planets – planet-star interactions

1 INTRODUCTION

One of the major surprises of exoplanet research is the discovery of “hot Jupiters” – giant planets in orbits of a few days (e.g., Mayor & Queloz 1995). It is yet unclear whether these planets formed in situ (Bodenheimer et al. 2000; Ikoma et al. 2001; Batygin et al. 2016; Boley et al. 2016), migrated inward due to interaction with a gaseous disk (Goldreich & Tremaine 1980; Lin et al. 1996), or are the result of tidal circularization of longer eccentric orbits of scattered planets (Rasio & Ford 1996).

Regardless of their formation mechanism, the orbits of many of the shortest-period hot Jupiters may shrink significantly within several Gyrs as a result of tidal dissipation in their host stars (e.g., Rasio et al. 1996). Eventually, these planets are expected to spiral in until they reach the Roche limit and begin to disintegrate. While a complete absorption of the planet by its host star is a possible outcome of the Roche-lobe overflow (e.g., Jackson et al. 2009; Metzger et al. 2012), recent studies suggest that, under some circumstances, hot Jupiters are only partially consumed, leaving behind lower-mass planets (Valsecchi et al. 2014, 2015; Jackson et al. 2016). Specifically, these studies find that the fate of an overflowing gas giant is dictated by the mass of its rocky core.

According to the popular core-nucleated accretion the-

ory, gas giants form as gas is gravitationally accreted onto a sufficiently massive rocky (or icy) core (Perri & Cameron 1974; Harris 1978; Mizuno et al. 1978; Mizuno 1980; Stevenson 1982). The critical core mass, around which a gas giant forms, has been the focus of intense theoretical study, with current estimates ranging from about $2M_\oplus$ to $30M_\oplus$, with M_\oplus denoting an Earth mass (Bodenheimer & Pollack 1986; Pollack et al. 1996; Ikoma et al. 2001; Rafikov 2006, 2011; Lee et al. 2014; Piso & Youdin 2014; Lee & Chiang 2015; Piso et al. 2015). Alternative planet formation theories do not require a core at all (Kuiper 1951; Cameron 1978; Boss 1997, 1998, 2000).

On the observational front, measurements of the gravitational field of the solar system’s oblate gas giants provides some constraints on their core mass, consistent with the theoretical estimates above (see Baraffe et al. 2014, for a review). In particular, coreless models are not excluded (Guillot et al. 1997; Saumon & Guillot 2004; Fortney & Nettelmann 2010).

Here, we utilize the critical role of dense cores in the evolution of overflowing gas giants to constrain the typical core mass of hot Jupiters. Explicitly, we compare the theoretical evolution of observed hot Jupiters that are expected to overflow and lose mass to the observed population of lighter planets (that may be the remnants of incomplete mass transfer), searching for an imprint of the core mass.

The outline of the paper is as follows. In Section 2 we investigate the hot Jupiters with the closest orbits, which are shrinking rapidly even more due to tidal dissipation. In

* E-mail: sivan.ginzburg@mail.huji.ac.il

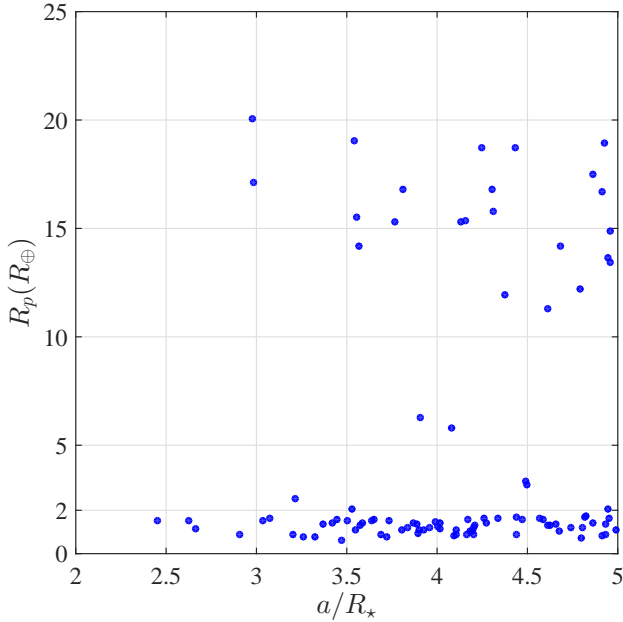


Figure 1. Observed planets from the exoplanets.org database (Han et al. 2014) with separations (in units of the stellar radius) $a/R_\star < 5$. Planets with radii $R_p > 10R_\oplus$ are Jupiters that are expected to spiral inward due to tidal dissipation within a few Gyrs, according to Equation (1). Error bars are typically of the order of 10% and are not displayed for clarity.

Section 3 we study the ensuing mass transfer, once these planets are sufficiently close to their host stars. In Section 4 we calculate the critical core mass, which determines the planet’s fate, and in Section 5 we characterize the surviving low-mass remnants of Roche-lobe overflow. Section 6 relates this work to previous studies and Section 7 summarizes our main conclusions.

2 INSPIRALLING HOT JUPITERS

Tides raised on a host star with radius R_\star and mass M_\star by a planet with mass M_p and separation a cause the planet’s orbit to decay on a time-scale

$$t_{\text{tide}} \equiv \frac{L}{|\dot{L}|} \sim \frac{a}{|\dot{a}|} = Q t_{\text{dyn}}^\star \left(\frac{a}{R_\star} \right)^{13/2} \frac{M_\star}{M_p} \quad (1)$$

$$\approx 4 \text{ Gyr} \left(\frac{a/R_\star}{5} \right)^{13/2} \frac{M_J}{M_p},$$

calculated by dividing the planet’s orbital angular momentum (which is transferred to the stellar spin) $L = M_p \sqrt{GM_\star a}$ by the tidal torque (given by, e.g., Goldreich & Soter 1966). $t_{\text{dyn}}^\star \equiv (G\rho_\star)^{-1/2} \approx 1 \text{ h}$ and ρ_\star denote the star’s dynamical time and density, respectively, G is Newton’s constant, and M_J is Jupiter’s mass. The numerical estimate is for a solar-like star and adopting a frequency-independent stellar tidal dissipation factor $Q \sim 10^6$ (see Essick & Weinberg 2016, and references therein). Tides raised on the planet keep it tidally locked, since a hot Jupiter’s synchronization time-scale is significantly shorter than t_{tide} above (Guillot et al. 1996).

In Fig. 1 we present observed planets with $a/R_\star < 5$. All the planets with radii $R_p > 10R_\oplus$ have masses $M_p \gtrsim M_J$

and will therefore spiral inward within their host star’s lifetime (the hosts are main-sequence stars), according to Equation (1). The discovery of several Jupiters with a/R_\star as low as 3, implying $t_{\text{tide}} \ll \text{Gyr}$, has led some authors to postulate a larger Q (Ogilvie & Lin 2007; Hellier et al. 2009; Penev & Sasselov 2011). Others remark, on the other hand, that dynamical scattering of Jupiters into short orbits (see Section 1) may repopulate these rapidly decaying orbits (e.g., Essick & Weinberg 2016). Additionally, a sample of hundreds of observed hot Jupiters would inevitably harbour a few short-lived planets, since Equation (1) predicts a detection probability of $\sim 1\%$ for $a/R_\star = 3$.

We conclude that there is an observed population of over a dozen hot Jupiters that are inspiralling with a time-scale $t_{\text{tide}} \lesssim \text{Gyr}$ (see also Essick & Weinberg 2016). Their typical mass is $\approx 1.4M_J$ and the typical radius is $\approx 1.4R_J$. By coincidence, the typical stellar and planetary densities are similar $\rho_\star \approx \rho_p \approx 0.6 \text{ g cm}^{-3}$. The low planetary density (relative to Jupiter) is a manifestation of the extensively-studied hot-Jupiter inflation puzzle (see, e.g., Spiegel & Burrows 2013; Ginzburg & Sari 2015, 2016, and references therein), which is also evident in Fig. 1. The low stellar density (relative to the Sun) reflects the typically higher mass of the host stars¹ $M_\star \approx 1.3M_\odot$ (see Torres et al. 2010, for a mass-radius relation). In the following sections we study the fate of such planets as they spiral towards their host stars.

3 STABLE ROCHE-LOBE OVERFLOW

As a planet inspirals towards its host star, it reaches the Roche limit at a separation

$$\frac{a}{R_\star} \simeq 2.4 \left(\frac{\rho_\star}{\rho_p} \right)^{1/3}, \quad (2)$$

where the numerical coefficient is suitable for an incompressible planet and it changes to $\simeq 2.0$ for compressible bodies (e.g. Rappaport et al. 2013, and references therein). Based on the interpolation between the two regimes in Rappaport et al. (2013) and Jupiter’s central to mean density ratio (e.g. Peebles 1964; Chabrier & Baraffe 2000), Equation (2) is accurate to within a few percent. As the planet loses mass through Roche-lobe overflow (RLO), the approximation improves since the planet becomes even less compressible (see Section 3.1).

Once the planet reaches the Roche limit, stable mass transfer may ensue, during which the planet remains on the verge of the Roche limit, given by Equation (2). The mass-loss and orbital evolution are driven by tidal angular momentum transfer, with a time-scale $\sim t_{\text{tide}}$, given by Equation (1). See Appendix A for a derivation and a discussion. See Metzger et al. (2012) for possibly observable transients in case the Roche limit lies within R_\star or if the mass transfer is unstable.

¹ $M_\star \approx 1.3M_\odot$ also marks the transition between stars with convective and radiative envelopes (Kraft 1967; van Saders & Pinsonneault 2013). Some studies suggest that stars with radiative envelopes have a significantly higher Q (Zahn 1977; Van Eylen et al. 2016). Considering this effect would roughly halve the number of inspiralling planets in Fig. 1.

3.1 Gas Compressibility

According to Equation (2), the planet's separation during RLO is simply a measure of its density $a \propto \rho_p^{-1/3}$. In this section we calculate ρ_p as a function of the planet's mass.

We first consider a zero-temperature coreless gas giant. The pressure inside such a planet is given by a simple equation of state (see, e.g., Padmanabhan 2001; Arras & Bildsten 2006; Ginzburg & Sari 2015)

$$P = K\rho_p^{5/3} \left[1 - \left(\frac{\rho_0}{\rho_p} \right)^{1/3} \right] = \beta GM_p^{2/3} \rho_p^{4/3}, \quad (3)$$

where the first term in brackets is due to electron degeneracy, with $K \sim h^2 m_e^{-1} m_p^{-5/3}$ (h is the Planck constant and m_e and m_p are the electron and proton masses), and the second term is due to electrostatic forces (ρ_0 is the zero-pressure density of cold gas). This pressure balances the one exerted by gravity $\sim GM_p^2/R_p^4$, which appears on the right hand side of Equation (3) with an order of unity constant β . We rewrite Equation (3) as

$$\left(\frac{\rho_p}{\rho_0} \right)^{1/3} = 1 + \left(\frac{M_p}{M_{\max}} \right)^{2/3}, \quad (4)$$

with $M_{\max} \equiv \beta^{-3/2} (K/G)^{3/2} \rho_0^{1/2}$. It is easy to see from Equation (4) that the planet's radius $R_p \propto (M_p/\rho_p)^{1/3} \propto M_p^{1/3} / [1 + (M_p/M_{\max})^{2/3}]$ peaks at $M_p = M_{\max}$, with $R_p \propto M_p^{1/3}$ for $M_p \ll M_{\max}$ and $R_p \propto M_p^{-1/3}$ for $M_p \gg M_{\max}$. We can easily calibrate $M_{\max} \simeq 3M_J$ from the peak in the radius-mass curves calculated in previous studies (Zapolsky & Salpeter 1969; Fortney et al. 2007). Equation (4) demonstrates that planets with a mass $M_p \ll M_{\max}$ are incompressible.

Next, we turn our attention to the low densities of observed hot Jupiters in comparison with cold gas giants (see Section 2). These low densities indicate that hot Jupiters retain high interior temperatures (e.g. Arras & Bildsten 2006), and may therefore deviate from the zero-temperature $\rho_p(M_p)$ relation of Equation (4). Specifically, the deviation in density is given by $d\rho/\rho = f(\theta)d\theta$, with θ denoting the degeneracy parameter, defined as the ratio of the ions' thermal pressure to the electrons' degeneracy pressure, and $f = -3/(1+\theta)$ (Ginzburg & Sari 2015). Consequently, the ratio of hot to cold densities $\rho(\theta)/\rho(\theta=0)$ is a function of θ alone. Guillot (2005) finds that θ is roughly uniform across a hot Jupiter's interior profile, because the pressure of both thermal ions and degenerate electrons scales as $P \propto \rho^{5/3}$. As a result, when the outer layers of a gas giant are removed through Roche-lobe overflow, the remaining planet retains its original θ , assuming the mass-loss is adiabatic (the thermal evolution time-scale of the planet's interior is longer than the orbital evolution for tidally evolving planets, i.e., below the dashed black line in Fig. 2 and 3; see Wu & Lithwick 2013; Ginzburg & Sari 2016).

We conclude that θ , and therefore the relative inflation $\rho_p(\theta)/\rho_p(\theta=0)$, is conserved during RLO. This result allows us to generalize Equation (4), which was derived for cold planets ($\theta=0$), to hot (inflated) planets ($\theta>0$), as they lose mass:

$$\rho_p^{1/3} \propto 1 + \left(\frac{M_p}{M_{\max}} \right)^{2/3}. \quad (5)$$

Notice that the density in Equation (5) is calibrated to a

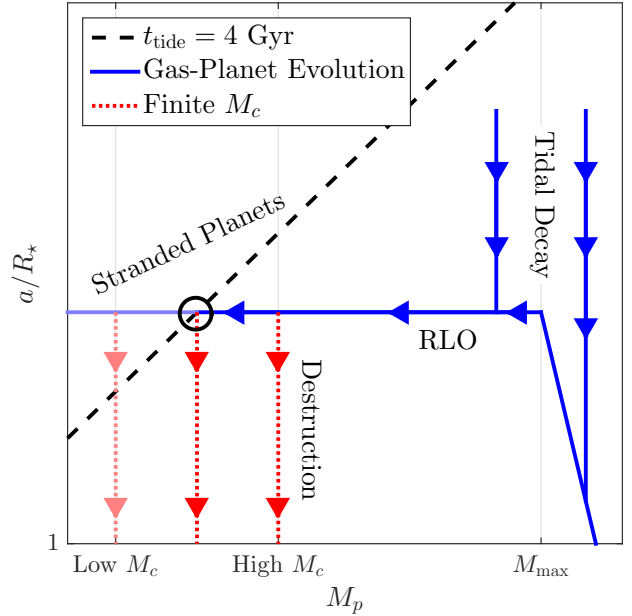


Figure 2. Schematic evolution of short-period hot Jupiters. Gas giants in short orbits inspiral towards the Roche limit at $a/R_* \approx 2.4$, given by Equation (2) with typical stellar and planetary densities. The ensuing Roche-lobe overflow (RLO) is at an approximately constant density for $M_c < M_p < M_{\max}$, according to Equation (5). When the planet is reduced to $M_p \sim M_c$, the density increases and the planet plunges towards the star (dotted red lines for three values of the core mass M_c). Planets with massive cores (rightmost dotted red line) are destroyed within a few Gyrs. Planets with lighter cores (pale lines) are stranded on the dashed black line, which marks the evolution time and is given by Equation (1).

lower value (i.e. lower than ρ_0 ; see Section 4 for a detailed calibration) in comparison with Equation (4), due to the inflation.

3.2 Asymptotic Trajectories

The stages of orbital evolution and mass loss are depicted schematically in Fig. 2 by considering the asymptotic behaviour of Equation (5). First, the planet's orbit decays until it reaches the Roche limit, at a separation $a/R_* \approx 2.4$, according to Equation (2), and substituting typical stellar and planetary densities (see Section 2). Next, the planet loses mass through RLO and its orbit evolves as $a \propto \rho_p^{-1/3}$. According to Equation (5), the density and therefore the separation of gas planets are approximately constant for $M_p \ll M_{\max}$. When the planet's mass becomes comparable to the mass of its dense core $M_p \sim M_c$, its mean density increases rapidly (see Section 4.1 for a more accurate analysis) as the atmosphere is lost, until $\rho_p = \rho_c$, with $\rho_c \approx 6 \text{ g cm}^{-3} (M_c/M_{\oplus})^{1/4}$ marking the rocky core's density (e.g. Valencia et al. 2006). According to Equation (2), the sudden increase in density causes the planet to plunge towards the star until $a/R_* \simeq 1$ and the planet is destroyed at the stellar surface.

As seen in Fig. 2, planets with massive cores (rightmost dotted red line) are destroyed within a few Gyrs. Planets with lighter cores (leftmost dotted red line), or without a

core (solid blue line), on the other hand, are stranded in a slow stable RLO (marked by a black circle). The gas mass fraction of these stranded planets is $M_{\text{atm}}/M_p \gtrsim 0.5$, because the descent towards the star begins when M_p is comparable to M_c , as explained above. By combining Equations (1) and (2) and substituting typical ρ_p and ρ_* (see Section 2) we estimate that the critical core mass (middle dotted red line) that distinguishes the two cases is a few M_{\oplus} .

The simple analysis above demonstrates how the typical hot-Jupiter core mass M_c can be inferred from the outcome of Roche-lobe overflow. If M_c is low then we expect to observe a population of gas rich ($\gtrsim 50\%$ in mass) super Earths at a separation $a/R_* \approx 2.4$. Such a population seems to be absent from the observations (see Section 5), implying that M_c is high. However, from Equations (1) and (2), the critical core mass is a sensitive function of the planet's density during RLO $M_c \propto \rho_p^{-13/6}$, necessitating a more accurate calculation.

4 CRITICAL CORE MASS

In Section 3.2 we identified a critical core mass M_c , which determines the outcomes of Roche-lobe overflow. Planets with heavier cores are destroyed by the star within a few Gyrs, while planets with lighter cores survive as short-period gas-rich super Earths. In this section we calculate the critical M_c more accurately. Explicitly, according to Equation (2), the planet's trajectory in the a - M_p plane is simply a function of the $\rho_p(M_p)$ relation. In Fig. 2 we approximated the density as constant for $M_c < M_p < M_{\text{max}}$, followed by a sharp increase for $M_p \simeq M_c$, resulting in simple trajectories. Here, we apply a realistic $\rho_p(M_p)$ relation, which takes into account the compressibility of the gas and the transition from a gas-dominated to a core-dominated planet, leading to more complex trajectories.

Fig. 3 displays the evolution of gas giants with realistic densities. The solid blue line, which is adequate for a coreless planet, is according to Equation (5), calibrated to a typical inspiralling hot Jupiter (i.e., using the coincidence $\rho_p = \rho_*$ for $M_p = 1.4M_J$; see Section 2). At the onset of RLO $M_p \approx M_J$ is comparable to $M_{\text{max}} \simeq 3M_J$. Therefore, as illustrated in Fig. 3, mass loss during RLO decompresses the planet according to Equation (5), causing its orbit to expand in consequence of Equation (2).

4.1 Dense Core

Finally, we consider planets with cores of a finite mass M_c and density ρ_c , engulfed by a gas atmosphere with a mass $M_{\text{atm}} \equiv M_p - M_c$ and density ρ_{atm} . The mean density ρ_p of such a two-layer planet is given by dividing M_p by the total volume, $M_c/\rho_c + M_{\text{atm}}/\rho_{\text{atm}}$:

$$\frac{\rho_p}{\rho_{\text{atm}}} = \frac{M_p/M_c}{\rho_{\text{atm}}/\rho_c + M_{\text{atm}}/M_c} \approx \frac{M_p}{M_{\text{atm}}}. \quad (6)$$

We consider envelopes that are massive enough to dominate the planet's volume $M_{\text{atm}}/M_c \gg \rho_{\text{atm}}/\rho_c$, and justify this assumption below. We see from Equation (6) that, for a roughly constant ρ_{atm} , the planet's density $\rho_p \propto M_p/(M_p - M_c)$ increases significantly when $M_p \sim M_c$, motivating the sharp increase in density there, used in our approximate

analysis in Section 3.2. However, as illustrated in Fig. 3 (dotted red lines), the gradual density increase implied by Equation (6) is translated to a gradual shrinkage of the orbit by Equation (2). This finer estimate of the density allows us to calculate the orbital evolution more accurately and to characterize the remnants of RLO (if there are any, see Section 3 and the discussion below) better.

To complete our realistic $\rho_p(M_p)$ relation, we substitute into Equation (6) $\rho_{\text{atm}}(M_{\text{atm}})$ from Equation (5), which describes the atmosphere's density for $M_{\text{atm}} \gtrsim M_c$. Although Equation (5) was derived for gaseous planets, it is valid for $M_{\text{atm}} \lesssim M_c$ as well. The reason is that, since $M_c \ll M_{\text{max}}$, ρ_{atm} is almost constant for $M_{\text{atm}} \sim M_c$, according to Equation (5). For $M_{\text{atm}} \lesssim M_c$ it is clear that the atmosphere is even less compressible (due to the weaker gravitational pressure), so ρ_{atm} is constant in that regime, as in Equation (5). With this substitution, our density-mass relation is

$$\rho_p^{1/3} \propto \left[1 + \left(\frac{M_{\text{atm}}}{M_{\text{max}}} \right)^{2/3} \right] \left(\frac{M_p}{M_{\text{atm}}} \right)^{1/3}, \quad (7)$$

which is again calibrated to $\rho_p = \rho_*$ for $M_p = 1.4M_J$ (this coincidence is explained in Section 2). The first term in Equation (7) accounts for the compression of the gas atmosphere for $M_{\text{atm}} \gtrsim M_{\text{max}} \gg M_c$ and approaches the zero-pressure density of the gas for $M_{\text{atm}} \lesssim M_c \ll M_{\text{max}}$ (as explained above, the exact form of this term is unimportant for $M_{\text{atm}} \lesssim M_c$). The second term describes the increase of the mean density, as the core becomes the dominant component, when $M_{\text{atm}} \lesssim M_c$. Essentially, Equation (7) is a trivial interpolation of these two regimes, which are uncoupled thanks to $M_c \ll M_{\text{max}}$. For a coreless planet $M_c = 0$, Equation (5) is reproduced.

Fig. 3 displays the orbital evolution of overflowing gas giants with densities given by Equation (7). The evolution is characterized by an orbital expansion that precedes the planet's final inspiral towards the star (see the caption of Fig. 3 for details). A similar behaviour was found in previous studies (Valsecchi et al. 2014, 2015; Jackson et al. 2016), and it is intuitively explained by the simpler Fig. 2. Quantitatively, our estimate of the critical core mass, above which planets are destroyed within a few Gyrs, is $M_c = 6M_{\oplus}$ (see Fig. 3). The properties of remnant planets (if $M_c < 6M_{\oplus}$) are described in Section 5.

4.2 Sensitivity to Q

The approximate analysis in Section 3.2, combined with Equation (1), yields a linear dependence of the critical core mass on the stellar tidal dissipation parameter $M_c \propto Q$. Fig. 3 illustrates that this linear relation is valid only approximately in the more elaborate calculation that we performed in this section, with $M_c/M_{\oplus} = 2$ and 14 for $Q = 3 \times 10^5$ and 3×10^6 , respectively.

Notice that for high Q values, not all the hot Jupiters in Fig. 1 will inspiral within a few Gyrs, as seen in Fig. 3. For low Q values, the remnant planets are less massive and their atmospheres are therefore susceptible to photo-evaporation (see Section 5).

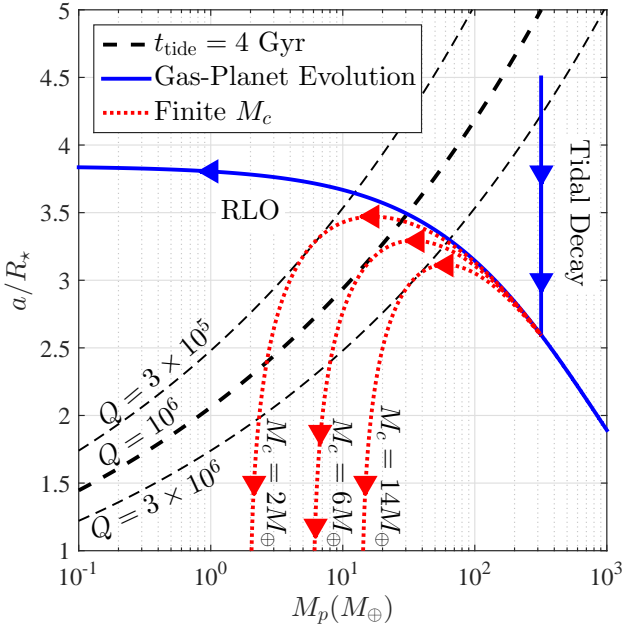


Figure 3. Same as Fig. 2, but with realistic densities $\rho_p(M_p)$, given by Equation (7), and inserted into Equation (2). The orbital evolution is plotted for core masses $M_c/M_\oplus = 2, 6, 14$ (dotted red lines, left to right) and for a coreless planet (solid blue line). During RLO, the density first decreases as gravitational pressure is lifted and then increases as the core becomes the dominant component. The minimum density is translated to a maximum separation, since $a \propto \rho_p^{-1/3}$. Planets with $M_c > 6M_\oplus$ are destroyed in a few Gyrs, assuming a nominal stellar tidal dissipation factor $Q = 10^6$ (thick middle dashed black line), while planets with lighter cores survive as “gas Neptunes” with $15M_\oplus < M_p < 30M_\oplus$ and $M_{\text{atm}}/M_p > 60\%$. The thin dashed black lines mark $Q = 3 \times 10^5$ and $Q = 3 \times 10^6$ (left to right) which correspond to critical core masses of $M_c/M_\oplus = 2$ and 14 .

5 REMNANT PLANETS

In Section 3 we demonstrated that hot Jupiters with light cores experience incomplete Roche-lobe overflow and survive as gas-rich lower mass planets. Using the results of Section 4, we can now characterize these surviving planets more accurately.

Fig. 3 shows that if $M_c < 6M_\oplus$, the planet’s evolution slows down, and it is stranded in RLO instead of plunging towards the star. Concretely, such planets appear in Fig. 3 between the solid blue line (no core) and the middle dotted red line ($M_c = 6M_\oplus$), with the leftmost dotted red line ($M_c = 2M_\oplus$) as an example. As seen in the figure, after a few Gyrs (i.e. on the thick middle dashed black line), these surviving planets constitute a very distinct population. Explicitly, all of them are expected to be “gas Neptunes” with masses $15M_\oplus < M_p < 30M_\oplus$ and $M_{\text{atm}}/M_p > 60\%$ (since $M_c < 6M_\oplus$), stranded at $a/R_* \approx 3.5$. The narrow range of remnant masses and separations is qualitatively explained by the simpler analysis in Section 3.2. The high gas fraction justifies our approximation $M_{\text{atm}}/M_c \gg \rho_{\text{atm}}/\rho_c \approx 3\%$ (see Section 4.1). According to Equation (6), this approximation breaks down when $\rho_p/\rho_{\text{atm}} \sim (M_p/M_c)/(\rho_{\text{atm}}/\rho_c) \approx \rho_c/\rho_{\text{atm}}$, i.e. when $\rho_p \approx \rho_c$, affecting only the lower parts of the dotted red

curves in Fig. 3 (at $a/R_* \approx 1$), which do not influence our results.

In addition to RLO, close-in planets lose mass through photo-evaporation by high-energy stellar radiation. While hot Jupiters lose only $\sim 1\%$ of their atmosphere during their lifetime (Murray-Clay et al. 2009), lighter super Earths can be stripped of their gas envelopes entirely (Lopez et al. 2012). By considering the high stellar flux $\propto (a/R_*)^{-2}$ and the intermediate mass of our remnant planets, their atmospheres should apparently be marginally unstable to evaporation (see Fig. 8 of Lopez & Fortney 2013, but with M_p instead of M_c , since $M_{\text{atm}} \gtrsim M_c$). However, since the stellar UV activity decreases rapidly afterwards, almost all of the mass loss occurs during the star’s first ~ 100 Myr (Lopez et al. 2012; Lopez & Fortney 2013; Owen & Wu 2013). The remnant planets that we consider here, on the other hand, reach their low mass only after Gyrs of tidal decay (as Jupiters, see Section 2). At this stage, the high-energy flux is too low to erode their atmospheres significantly (see Fig. 1 of Lopez & Fortney 2013). We conclude that the remnant gas Neptunes retain their heavy atmospheres despite the high incident stellar flux that they receive (see also the discussion in Section 6).

Even without detailed modelling of the structure and thermal evolution (after a planet is stranded, its thermal evolution may become faster than its tidal evolution, so it is no longer adiabatic) of gas Neptunes, it is clear that their radii are expected to be in the range $5 - 10R_\oplus$ (Zapolsky & Salpeter 1969; Fortney et al. 2007; Lopez et al. 2012). This range is remarkably empty, as seen in Fig. 1. Moreover, one of the two planets in the range appears to be a disintegrating sub-Earth (Rappaport et al. 2012); the other orbits an exceptionally low-density star (Morton et al. 2016), implying, according to Equation (2), a significantly smaller separation, if it were an RLO remnant.

In summary, gas Neptunes, which are the expected remnants of incomplete RLO of hot Jupiters, are absent from the observations. We therefore come to the conclusion that the majority of hot-Jupiter cores have a mass $M_c > 6M_\oplus$. In this case, the planets complete the RLO and do not leave a remnant, as seen in Fig 3. Although a statistical analysis of the chance to observe non-stranded ($M_c > 6M_\oplus$) overflowing planets (analogous to the analysis in Penev et al. 2012, for inspiralling Jupiters) is beyond the scope of this work, it is clear that such an analysis would only increase our lower limit on M_c . The reason is that even planets with cores somewhat heavier than $6M_\oplus$ spend a long time close to the thick black dashed line in Fig. 3, where the tidal evolution time is long, and there is a non-negligible chance to observe them, yet none are observed. Finding a large population of close-orbiting gas Neptunes would have reversed our conclusion, though additional formation channels (rather than RLO of hot Jupiters) should also be considered in this case.

6 RELATION TO PREVIOUS WORKS

In this section we outline the main differences between this work and previous studies of the Roche-lobe overflow of hot Jupiters.

First and foremost, the goal of our study is different. Previous works (Valsecchi et al. 2014, 2015; Jackson et al.

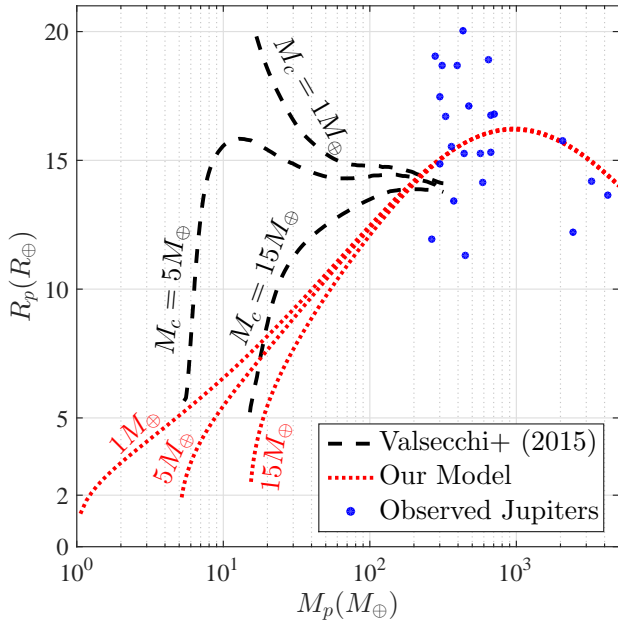


Figure 4. Mass-radius relation for overflowing Jupiters with different core masses ($M_c/M_\oplus = 1, 5, 15$, as labelled). The population of observed inspiralling Jupiters (blue dots) is from Fig. 1. The dashed black lines are from Figure 7 of Valsecchi et al. (2015), while the dotted red lines are according to Equation (7). The contrast between the two models is explained by two main differences: (i) We account for inflation due to deep heating, which is absent from Valsecchi et al. (2015). (ii) In Valsecchi et al. (2015), planets that are reduced to a low mass are re-inflated (reheated) by the stellar irradiation, while we assume that the overflow is adiabatic (following Wu & Lithwick 2013; Ginzburg & Sari 2016). Our models are truncated when the approximation $M_{\text{atm}}/M_c \gg \rho_{\text{atm}}/\rho_c$ breaks down (see Section 4.1).

2016) studied the correlations between the mass and the period of mainly-rocky super Earths and checked whether these could be the surviving cores of hot Jupiters that underwent RLO. Here, we argue that none of the observed super Earths were produced by RLO. Instead, we constrain the hot-Jupiters’ core mass by the absence of more massive low-density “gas Neptunes” (see Section 5).

Another major difference is our method. Previous studies employed rather complex mass-radius relations and calculated the orbital evolution numerically using the MESA code. We, on the other hand, address the problem with a simpler analytical approach, allowing us to intuitively draw qualitative and quantitative conclusions and to easily test the parameter space (see Section 4.2). We did not introduce any severe approximations, so our analytical method does not restrict our accuracy.

Putting these differences aside, many of our results qualitatively reproduce previous conclusions. For instance, both Valsecchi et al. (2014) and Jackson et al. (2016) notice that there are no gas-rich planets currently at RLO, leading Valsecchi et al. (2014) to conclude that most hot Jupiters have rocky cores. Here, we take this conclusion one step further and constrain the core mass more accurately. Similarly, Valsecchi et al. (2015) and Jackson et al. (2016) find that planets may be stranded near a maximum period that is

anti-correlated with their core mass, as in Fig. 3. Nonetheless, we list below several critical quantitative differences:

(i) *Mass-radius relation.* The previous studies refer to a variety of mass-radius relations for irradiated planets, taken from earlier numerical planetary evolution models (Fortney et al. 2007; Batygin & Stevenson 2013; Lopez & Fortney 2014). However, all of these models evolve planets at a constant M_p for a few Gyrs. The cooling of lighter planets is hindered more by stellar irradiation; hence the degeneracy parameter θ (see Section 3.1) and the relative inflation scale inversely with M_p in the models (see Wu & Lithwick 2013; Ginzburg & Sari 2016). Overflowing planets, on the other hand, retain their original small θ , which corresponds to a few Gyrs evolution of the original Jupiter mass, as explained in Section 3.1. As a result, using the models above flattens the $R_p(M_p)$ relation and steepens the $\rho_p(M_p)$ curve for $M_p \lesssim M_J$. Consequently, using Equation (2), Valsecchi et al. (2014), who incorporate the models of Fortney et al. (2007) and Batygin & Stevenson (2013), overestimate the orbital expansion at the onset of RLO (see Fig. 3). More recent studies (Valsecchi et al. 2015; Jackson et al. 2016) calculate the mass-radius relation during RLO directly, using MESA. In Fig. 4 we compare our mass-radius relation to Valsecchi et al. (2015). The contrast between the two models is explained by two main differences. First, our model accounts for inflation due to deep heating (such as Ohmic dissipation, see Batygin & Stevenson 2010), which is absent from Valsecchi et al. (2015), despite being necessary in order to explain the large radii of observed hot Jupiters. Second, the overflowing planets in Valsecchi et al. (2015) are re-inflated (reheated) to low densities by the stellar irradiation as they lose mass, contrary to numerical (Wu & Lithwick 2013) and analytical (Ginzburg & Sari 2016) studies that find prohibitively long re-inflation time-scales. The origin of the discrepancy (for $M_p \sim M_J$) between Valsecchi et al. (2015) and Wu & Lithwick (2013), who also use MESA, is unclear, nor is it explained in Valsecchi et al. (2015). Our analytical estimates (Ginzburg & Sari 2016) agree better with Wu & Lithwick (2013). However, since both Wu & Lithwick (2013) and Ginzburg & Sari (2016) focus on roughly Jupiter-mass planets, the re-inflation time for significantly lower masses might be shorter. Another possibility is that θ is not conserved even during adiabatic mass-loss due to deviations from the $P \propto \rho^{5/3}$ scaling (see Section 3.1). From Fig. 3, such re-inflation would only increase our lower bound on M_c by increasing the separation at low M_p values. The low densities in Valsecchi et al. (2015) result in an overestimate of the orbital expansion during RLO (see also Jackson et al. 2016). Moreover, the increase in R_p as the planet loses mass (see Fig. 4) has a destabilizing effect, leading Valsecchi et al. (2015) to consider unstable mass-transfer, while we find that the mass transfer is stable (see Appendix A).

(ii) *Photo-evaporation.* As explained in Section 5, a combination of the high mass ($M_p > 15M_\oplus$) of remnant planets and the late stage of stellar evolution ($\gg 100$ Myr), in which they are reduced to this mass, renders photo-evaporation (PE) irrelevant for Roche-lobe overflow. While Valsecchi et al. (2014) and Jackson et al. (2016) ignore PE as well, Valsecchi et al. (2015) incorporate it in their MESA runs. They find that PE removes a significant portion of

a remnant gas-Neptune’s atmosphere in a few Gyrs. According to Section 5, this result is at odds with the results of Lopez & Fortney (2013), considering the planet’s separation, mass, and age. Using the results of Lopez & Fortney (2013), we estimate that only a minor part of a gas Neptune’s mass (no more than a few M_{\oplus}) is removed by PE. In fact, this difference is also evident in Fig. 2 of Valsecchi et al. (2015), which compares their PE prescription to Lopez & Fortney (2013). Despite apparent similarities, the figure reveals that the prescription of Valsecchi et al. (2015) removes ≈ 3 times the mass, in comparison with Lopez & Fortney (2013), at late times (\gtrsim Gyr) which are relevant for our scenario. This modest difference is enough to explain the dissimilar end-results of PE (gas Neptunes vs. rocky super-Earths with $M_{\text{atm}} \ll M_c$).

7 CONCLUSIONS

More than a dozen observed hot Jupiters will inevitably inspiral towards their host stars within a few gigayears, due to tidal interaction (see Fig. 1). At some stage, they will reach the Roche limit and start losing mass via Roche-lobe overflow (RLO). Capitalizing on previous works, these doomed planets can serve as a laboratory to study the structure of hot Jupiters. In particular, their evolution during RLO critically depends on their core mass M_c (Valsecchi et al. 2014, 2015; Jackson et al. 2016).

Here, we characterized this population of inspiralling Jupiters and affirmed that their mass overflow is stable, with a rate determined by the tidal evolution time-scale t_{tide} . We identified two possible RLO outcomes:

- (i) $M_c < 6M_{\oplus}$: The planet’s mass decreases until $t_{\text{tide}} \gtrsim$ Gyr, stranding the remnant planet (which is reduced to a mass $15M_{\oplus} < M_p < 30M_{\oplus}$) at a separation $a/R_{\star} \approx 3.5$.
- (ii) $M_c > 6M_{\oplus}$: The planet’s atmosphere is gradually removed, until the dense core increases the planet’s mean density ρ_p . During RLO, $a \propto \rho_p^{-1/3}$, causing the orbit to shrink until the planet quickly crushes on the stellar surface.

The remnants in option (i) should have been Neptune mass planets, composed primarily of gas. Owing to a combination of their relatively high mass and the late stage in stellar evolution at which they are reduced to this mass, these “gas Neptunes” are not affected by photo-evaporation, in contrast to lighter super Earths (Lopez et al. 2012; Lopez & Fortney 2013; Owen & Wu 2013). Surviving gas Neptunes would have a distinct imprint on the observations as $5 - 10R_{\oplus}$ planets at $a/R_{\star} \approx 3.5$. However, such planets are remarkably absent from the transiting population (see Fig. 1).

The lack of short-period gas Neptunes, compared with the relative abundance of their possible progenitors (inspiralling Jupiters) leads us to the conclusion that option (ii) is the prevalent scenario, i.e., the typical hot-Jupiter core mass satisfies $M_c > 6M_{\oplus}$. This constraint is similar to modern theoretical estimates of the minimum M_c required for Jupiter formation by the core-accretion scenario (Lee & Chiang 2015; Piso et al. 2015). However, observations and alternative formation theories do not rule out lighter cores or coreless planets (Boss 2000; Baraffe et al. 2014). Therefore, the indirect

observational evidence that is presented in this work provides a useful lower limit on the core mass, which may help to establish the core-accretion theory.

We employ a simple mass-density relation, enabling us to solve the planet’s orbital evolution analytically. Despite its simplicity, our analytical $\rho_p(M_p)$ function, given by Equation (7), fully incorporates the two-layer (core and gas) structure of the planet, the compressibility of these layers, and the inflation due to stellar irradiation. Accuracy is achieved by a simple calibration to numerical mass-radius relations and to the observations. Using this density function, we reproduced the complex trajectories of overflowing planets in the $a - M_p$ plane. Specifically, planets first decompress as the gravitational pressure is lifted, and then increase in mean density as their dense core becomes the dominant component. Since $a \propto \rho_p^{-1/3}$, this minimum in ρ_p is translated to a maximum separation (see also Valsecchi et al. 2014, 2015; Jackson et al. 2016). Our analytical approach allows us to easily test our assumptions and sensitivity to the various parameters.

Several aspects of our model deserve further attention, which we leave to future work:

- (i) The results depend on the poorly-known stellar tidal dissipation parameter Q (see Section 4.2). A more accurate Q value would secure our conclusions. Alternatively, given an estimate of M_c (e.g. from core-accretion theory), our results may be used to constrain $Q/10^6 \lesssim M_c/(6M_{\oplus})$. Notice, however, that a high $Q > 10^7$ is also consistent with our findings, because in that case most of the Jupiters in Fig. 1 will not inspiral towards the Roche limit, according to Equation (1). In this scenario, the lack of observed RLO remnants merely reflects the scarcity of their possible progenitors.
- (ii) The planet’s evolution during RLO is essentially a reflection of its density $\rho_p(M_p)$. Therefore, a more accurate calculation, involving a sophisticated equation of state, can improve our constraint (see, however, Section 6).
- (iii) While gas Neptunes are unaffected by photo-evaporation (PE), lighter planets are more vulnerable. Such super Earths, which may be the result of RLO with low Q values, necessitate an analysis of PE during their late evolution. In addition, it is crucial to reconcile the difference between the PE prescriptions of Lopez & Fortney (2013) and Valsecchi et al. (2015) at late times.

In summary, by identifying the (missing) remnants of inspiralling hot Jupiters that undergo Roche-lobe overflow, we were able to constrain their core mass. This constraint may be used to distinguish between different formation scenarios of gas giants. Moreover, our analysis shows that short-period low-density super Earths cannot be the result of RLO of inspiralling Jupiters, unless Q is low. Instead, these planets could have formed by core-accretion that did not reach the runaway phase, as their atmosphere mass fractions $M_{\text{atm}}/M_c \lesssim 0.5$ suggest (see, e.g., Ginzburg et al. 2016; Lee & Chiang 2016, and references therein).

ACKNOWLEDGEMENTS

This research was partially supported by ISF (Israel Science Foundation) and iCore (Israeli Centers of Research

Excellence) grants. This research has made use of the Exoplanet Orbit Database and the Exoplanet Data Explorer at exoplanets.org. We thank Kenta Hotokezaka, Itai Linial, and Brian Metzger for discussions and comments and Brian Jackson for a comprehensive review that improved the paper.

REFERENCES

- Arras P., Bildsten L., 2006, *ApJ*, **650**, 394
- Baraffe I., Chabrier G., Fortney J., Sotin C., 2014, *Protostars and Planets VI*, pp 763–786
- Batygin K., Stevenson D. J., 2010, *ApJ*, **714**, L238
- Batygin K., Stevenson D. J., 2013, *ApJ*, **769**, L9
- Batygin K., Bodenheimer P. H., Laughlin G. P., 2016, *ApJ*, **829**, 114
- Bodenheimer P., Pollack J. B., 1986, *Icarus*, **67**, 391
- Bodenheimer P., Hubickyj O., Lissauer J. J., 2000, *Icarus*, **143**, 2
- Boley A. C., Granados Contreras A. P., Gladman B., 2016, *ApJ*, **817**, L17
- Boss A. P., 1997, *Science*, **276**, 1836
- Boss A. P., 1998, *ApJ*, **503**, 923
- Boss A. P., 2000, *ApJ*, **536**, L101
- Cameron A. G. W., 1978, *Moon and Planets*, **18**, 5
- Chabrier G., Baraffe I., 2000, *ARA&A*, **38**, 337
- Essick R., Weinberg N. N., 2016, *ApJ*, **816**, 18
- Fortney J. J., Nettelmann N., 2010, *Space Sci. Rev.*, **152**, 423
- Fortney J. J., Marley J. S., Barnes J. W., 2007, *ApJ*, **659**, 1661
- Ginzburg S., Sari R., 2015, *ApJ*, **803**, 111
- Ginzburg S., Sari R., 2016, *ApJ*, **819**, 116
- Ginzburg S., Schlichting H. E., Sari R., 2016, *ApJ*, **825**, 29
- Goldreich P., Soter S., 1966, *Icarus*, **5**, 375
- Goldreich P., Tremaine S., 1980, *ApJ*, **241**, 425
- Guillot T., 2005, *Annual Review of Earth and Planetary Sciences*, **33**, 493
- Guillot T., Burrows A., Hubbard W. B., Lunine J. I., Saumon D., 1996, *ApJ*, **459**, L35
- Guillot T., Gautier D., Hubbard W. B., 1997, *Icarus*, **130**, 534
- Han E., Wang S. X., Wright J. T., Feng Y. K., Zhao M., Fakhouri O., Brown J. I., Hancock C., 2014, *PASP*, **126**, 827
- Harris A. W., 1978, in *Lunar and Planetary Science Conference*, pp 459–461
- Hellier C., et al., 2009, *Nature*, **460**, 1098
- Ikoma M., Emori H., Nakazawa K., 2001, *ApJ*, **553**, 999
- Jackson B., Barnes R., Greenberg R., 2009, *ApJ*, **698**, 1357
- Jackson B., Jensen E., Peacock S., Arras P., Penev K., 2016, *Celestial Mechanics and Dynamical Astronomy*, **126**, 227
- Kraft R. P., 1967, *ApJ*, **150**, 551
- Kuiper G. P., 1951, *Proceedings of the National Academy of Science*, **37**, 1
- Lee E. J., Chiang E., 2015, *ApJ*, **811**, 41
- Lee E. J., Chiang E., 2016, *ApJ*, **817**, 90
- Lee E. J., Chiang E., Ormel C. W., 2014, *ApJ*, **797**, 95
- Lin D. N. C., Bodenheimer P., Richardson D. C., 1996, *Nature*, **380**, 606
- Linial I., Sari R., 2017, in prep.
- Lopez E. D., Fortney J. J., 2013, *ApJ*, **776**, 2
- Lopez E. D., Fortney J. J., 2014, *ApJ*, **792**, 1
- Lopez E. D., Fortney J. J., Miller N., 2012, *ApJ*, **761**, 59
- Mayor M., Queloz D., 1995, *Nature*, **378**, 355
- Metzger B. D., Giannios D., Spiegel D. S., 2012, *MNRAS*, **425**, 2778
- Mizuno H., 1980, *Progress of Theoretical Physics*, **64**, 544
- Mizuno H., Nakazawa K., Hayashi C., 1978, *Progress of Theoretical Physics*, **60**, 699
- Morton T. D., Bryson S. T., Coughlin J. L., Rowe J. F., Ravichandran G., Petigura E. A., Haas M. R., Batalha N. M., 2016, *ApJ*, **822**, 86
- Murray-Clay R. A., Chiang E. I., Murray N., 2009, *ApJ*, **693**, 23
- Ogilvie G. I., Lin D. N. C., 2007, *ApJ*, **661**, 1180
- Owen J. E., Wu Y., 2013, *ApJ*, **775**, 105
- Padmanabhan T., 2001, *Theoretical Astrophysics - Volume 2, Stars and Stellar Systems*
- Peebles P. J. E., 1964, *ApJ*, **140**, 328
- Penev K., Sasselov D., 2011, *ApJ*, **731**, 67
- Penev K., Jackson B., Spada F., Thom N., 2012, *ApJ*, **751**, 96
- Perri F., Cameron A. G. W., 1974, *Icarus*, **22**, 416
- Piso A.-M. A., Youdin A. N., 2014, *ApJ*, **786**, 21
- Piso A.-M. A., Youdin A. N., Murray-Clay R. A., 2015, *ApJ*, **800**, 82
- Pollack J. B., Hubickyj O., Bodenheimer P., Lissauer J. J., Podolak M., Greenzweig Y., 1996, *Icarus*, **124**, 62
- Rafikov R. R., 2006, *ApJ*, **648**, 666
- Rafikov R. R., 2011, *ApJ*, **727**, 86
- Rappaport S., Joss P. C., Webbink R. F., 1982, *ApJ*, **254**, 616
- Rappaport S., et al., 2012, *ApJ*, **752**, 1
- Rappaport S., Sanchis-Ojeda R., Rogers L. A., Levine A., Winn J. N., 2013, *ApJ*, **773**, L15
- Rasio F. A., Ford E. B., 1996, *Science*, **274**, 954
- Rasio F. A., Tout C. A., Lubow S. H., Livio M., 1996, *ApJ*, **470**, 1187
- Saumon D., Guillot T., 2004, *ApJ*, **609**, 1170
- Spiegel D. S., Burrows A., 2013, *ApJ*, **772**, 76
- Stevenson D. J., 1982, *Planet. Space Sci.*, **30**, 755
- Torres G., Andersen J., Giménez A., 2010, *A&ARv*, **18**, 67
- Valencia D., O’Connell R. J., Sasselov D., 2006, *Icarus*, **181**, 545
- Valsecchi F., Rasio F. A., Steffen J. H., 2014, *ApJ*, **793**, L3
- Valsecchi F., Rappaport S., Rasio F. A., Marchant P., Rogers L. A., 2015, *ApJ*, **813**, 101
- Van Eylen V., Winn J. N., Albrecht S., 2016, *ApJ*, **824**, 15
- Wu Y., Lithwick Y., 2013, *ApJ*, **763**, 13
- Zahn J.-P., 1977, *A&A*, **57**, 383
- Zapolsky H. S., Salpeter E. E., 1969, *ApJ*, **158**, 809
- van Saders J. L., Pinsonneault M. H., 2013, *ApJ*, **776**, 67

APPENDIX A: OVERFLOW STABILITY

The stability and rate of the Roche-lobe overflow, once the Roche limit is reached and the planet starts to lose mass ($dM_p < 0$), is based on Rappaport et al. (1982), with a brief description here (see also Valsecchi et al. 2014, 2015; Jackson et al. 2016).

In the absence of tides, the orbital angular momentum $L = M_p \sqrt{GM_* a}$ is conserved (though see the discussion below) during mass transfer, so that $d \ln a = -2 d \ln M_p$. The expanding orbit and the shrinking mass change the planet’s Roche-lobe radius $R_L \sim a(M_p/M_*)^{1/3}$. Specifically, $d \ln R_L = d \ln a + (1/3) d \ln M_p = -(5/3) d \ln M_p$. The response of the planet’s radius to the mass loss is given by its mass-radius relation, parametrized by $\xi \equiv d \ln R_p / d \ln M_p$. When the planet reaches the Roche limit, $R_p = R_L$ by definition, as realized in Equation (2). Therefore, the sign of $d \ln R_L - d \ln R_p = -d \ln M_p (5/3 + \xi)$ determines whether the mass transfer causes the planet to overflow its Roche lobe even more (triggering unstable mass transfer) or whether it shuts down the overflow. For gas giants $\xi > -1/3$ (see Section 3.1), promoting stable mass transfer. When tides, or any other orbital angular momentum loss mechanism (e.g. gravitational waves) are included, the stable mass transfer

ensures that the planet is kept on the verge of overflow, so that $R_p = R_L$, and Equation (2) is satisfied. Moreover, by adding angular momentum loss to the analysis above, we find that $2d\ln L = (5/3 + \xi)d\ln M_p$, implying that the Roche-lobe overflow time-scale is determined by Equation (1).

These results are easily generalized for a non-conservative mass transfer scenario, in which a fraction of the mass escapes from the star-planet system with a fraction of its orbital angular momentum $d\ln L_{\text{mass-loss}} \equiv \alpha d\ln M_p$. In this case, the mass-transfer rate is given by

$$\frac{|\dot{M}_p|}{M_p} = \left(\frac{2}{5/3 + \xi - 2\alpha} \right) t_{\text{tide}}^{-1}, \quad (\text{A1})$$

where the rate of orbital angular momentum loss by tides is given by Equation (1), and where the stability criterion is $5/3 + \xi - 2\alpha > 0$. As noted by Metzger et al. (2012) and Jackson et al. (2016), even if no mass is lost from the system, α can be as large as $\sqrt{R_*/a}$ because the accreted mass can transfer orbital angular momentum to the spin of the star. Using Equation (2) with the coincidence $\rho_p \approx \rho_*$ (see Section 2) and $\xi \approx 1/3$ (for a roughly constant density, which is adequate for $M_c < M_p < 3M_J$, as explained in Section 3), we conclude that the mass transfer is stable if less than about a third of the mass escapes the system (or if it does not carry with it its entire original angular momentum). When $M_p \sim M_c$, the density and therefore $\sqrt{R_*/a}$ increase (see Sections 3 and 4), but $\xi \approx M_p/(3M_{\text{atm}})$ increases more dramatically, so the mass transfer remains stable.

To summarize, the Roche-lobe overflow is stable, unless the mass transfer is highly non-conservative. Determining the amount of mass and angular momentum loss from the system is beyond the scope of this work (see, e.g., Linial & Sari 2017), so we follow previous studies and assume a stable overflow.

This paper has been typeset from a $\text{\TeX}/\text{\LaTeX}$ file prepared by the author.